# Comparing Three Spaceborne Optical Sensors via Fine Scale Pixel-based Urban Land Cover Classification Products

André Breytenbach[1] , Corné Eloff[2], Erika Pretorius[3]

[1]Built Environment, Council for Scientific and Industrial Research ABreytenbach@csir.co.za
[2] Built Environment, Council for Scientific and Industrial Research
[3]Centre for Geoinformation Science, Geography, Geoinformatics and Meteorology, University of Pretoria

## Abstract

*Accessibility to higher resolution earth observation satellites suggests an improvement in the potential for fine scale image classification. In this comparative study, imagery from three optical satellites (WorldView-2, Pléiades and RapidEye) were used to extract primary land cover classes from a pixel-based classification principle in a suburban area. Following a systematic working procedure, manual segmentation and vegetation indices were applied to generate smaller subsets to in turn develop sets of ISODATA unsupervised classification maps. With the focus on the land cover classification differences detected between the sensors at spectral level, the validation of accuracies and their relevance for fine scale classification in the built-up environment domain were examined. If an overview of an urban area is required, RapidEye will provide an above average (0.69 κ) result with the built-up class sufficiently extracted. The higher resolution sensors such as WorldView-2 and Pléiades in comparison delivered finer scale accuracy at pixel and parcel level with high correlation and accuracy levels (0.65-0.71 κ) achieved from these two independent classifications.*

## 1. Introduction

Since 1999, with the launch of the first 1m panchromatic ground sample distance (GSD) commercial earth observation satellite, IKONOS, the potential for fine scale classification from satellite imagery improved significantly. Very high resolution (VHR) earth observation satellites cover the dominant solar-reflectance electromagnetic spectrum values, especially in the visible (0.4µm – 0.7µm) and near infrared (NIR, 0.7µm – 1.1µm) ranges. Traditional multispectral satellites such as IKONOS (4m), QuickBird (2.4m) and now Pléiades (2m) provide four spectral bands within the visible and NIR range. DigitalGlobe, operator and owner of the WorldView-2 (2m) satellite introduced a total of eight multi-spectral bands within the visible and NIR spectrum range. Modern remote sensing (RS) technology – as opposed to costly and time consuming in-field observations and surveys – for the classification and extraction of thematic information such as land cover/land use (LC/LU) within urban environments, has shown great promise over this past decade (Brito and Quintanilha, 2012).

Other than the unique nature of remotely sensed imagery (spectral composition, GSD, etc.), it is also the availability of suitable training samples, the choice of classification method and the definition of the desired target classes that are the main factors that may affect the accuracy of remotely sensed data classification (Lu and Weng, 2007). In principle, three types of classification methods exist, namely unsupervised, supervised and hybrid. Unsupervised classification clusters pixels in a dataset based on statistics only, without any user-defined training classes. The most commonly used unsupervised LC/LU classifier is the Iterative Self-Organizing Data Analysis (ISODATA) classification algorithm (Tou & Gonzalez, 1974). It is used to create a user-defined number of clusters or classes in an image that must later be labelled by the analyst to create geo-information, e.g. a thematic map. On the other hand, several types of statistics-based supervised classification algorithms have been developed and are included in various remote sensing (RS) software systems and geographic information systems (GIS) today. Examples of the more popular classifiers (in increasing complexity) are parallelepiped, minimum distance, maximum likelihood (MLC), and Mahalanobis distance (Richards, 1999; Xiang *et al*., 2005). With supervised statistical classification algorithms the analyst must first locate and define samples (training areas) in the image for each specified class. The algorithm then compares each pixel in the image with the different training areas to determine which training area best correlates to the pixel in question and once discovered, the image pixel is labelled with the corresponding class. Hybrid methods can combine the advantages of manual, parametric and non-parametric methods in various combinations to optimise the classification process (Lu *et al*., 2010).

As an alternative to parametric classifiers, other research has made use of non-parametric methods such as artificial neural networks, binary decision trees (DT) and discriminant analysis (DA) to produce functional land cover products (Heinl *et al*., 2009; Fröhlich *et al*., 2013; Li *et al.*, 2013). Baraldi *et al*. (2010) demonstrated that an operational automatic pixel-based near-realtime four-band IKONOS-like Spectral Rule-based decision tree Classifier (ISRC) is eligible for use in operational VHR spaceborne measurement systems such as those envisaged under the on-going international programs such as Global Monitoring for the Environment and Security and Global Earth Observation System of Systems. Geographic object-based image analysis (GEOBIA), as opposed to pixel-based image processing, is also emerging as a popular classification method (Thunig *et al*., 2011; Tehrany *et al*., 2013). The process involves segmentation during which the pixels in an image are grouped into homogeneous interlocking regions as resolved by a specific segmentation algorithm (Myburgh and Van Niekerk, 2013). The segmented image can then be classified at the segment level instead of the pixel level. Its ability to incorporate contextual information and ancillary data (e.g. elevation/height models) makes GEOBIA suitable for the integration of various additional features for image classification (Wurm *et al*., 2009; Aguilar *et al*., 2012; Salehi *et al*., 2012). To improve accuracy even further with regards to urban land cover classification, some researchers successfully combined a pixel-based classifier with GEOBIA as another type of hybrid method (Bouziani *et al*., 2010; Elsharkawy *et al*., 2012). For example, LC classification in a complex urban-rural landscape with Quickbird imagery was performed by Moran

(2010) using Extraction and Classification of Homogeneous Objects (ECHO), a multistage spectral-spatial classifier that combines spectral and spatial/textural features (Biehl and Landgrebe, 2002) that also incorporates MLC, followed by segmentation-based classification. Huth *et al*. (2012) introduced the concept and implemented a methodology to classify multi-spectral and multi-temporal RS imagery within an automated processing environment, named TWinned Object and Pixel based Automated Classification Chain (TWOPAC). Available as an Open Source application, TWOPAC adopted classification routines founded on both pixel-based classification and object-based characteristics (*e.g.* shape parameters), as well as object statistics, by following a novel DT approach.

With the advantage of available (archived) temporal datasets and by means of the integration of RS and GIS techniques it is possible to analyse and classify the changing pattern of land cover over different periods (Kennedy *et al*., 2009). This in turn allows the analyst to better understand the dynamic changes that have occurred during that time within the area of interest. Change detection analysis can basically be grouped into two categories: (1) those detecting binary change/non-change information and (2) those detecting a detailed 'from-to' change trajectory (Lu *et a*l., 2004). The first group of techniques can include using image differencing, vegetation index differencing, and principal component analysis (PCA), whereas the second group can make use of the post-classification comparison (map-to-map comparison), multidate classification (image-to-image comparison) and hybrid change detection methods (Lu *et al*., 2010). In the first case, simple raster calculations between the specific imagery of different dates using the spectral or derived pixel values are normally performed. PCA is a mathematical technique for reducing the dimensionality of a data set (Jackson, 1983) and two PCA approaches to RS can be used in change detection (Muchoney & Haack, 1994). The first, merged data transformation, is an approach that registers and treats all the bands from the n-dimensional multi-temporal image data set as a single N-dimensional data set as input to the PCA (Munyati, 2004). Independent data transformation analysis, the second approach, uses PCA to spectrally enhance each individual image in a multi-temporal dataset and then classify each image separately for use in post classification change detection (Gholami *et al*., 2012). Post-classification comparison allows the analyst to determine the difference between independently classified images from each of the dates in question, making it the preferred method in which "from" and "to" classes can be calculated automatically for each changed pixel (Serra *et al*., 2003). The application of landscape metrics (using FRAGSTATS software, for example) is also useful to measure and analyze the temporal urban land cover changes and urban sprawl phenomenon from the classified images (Alexakis *et al*., 2012; Fichera *et al*., 2012).

The built environment domain is a complex field where the dynamics between rural and urbanised areas require fine scale geo-information to determine micro elements of importance to town planning. Aggregated land cover and/or land use classes could result in the misinterpretation of that spatial landscape and the actual area coverage of dominant classes. VHR imagery holds the potential to distinguish specific land cover types within a stand parcel as the smallest administrative unit in the cadastre boundary. As the basis for categorisation, a systematic pixel-based classification

technique utilizing the spectral pattern that characterises the data per pixel (Martinfar *et al*., 2007) was applied in this work. The focus was on the land cover classification differences detected between three selected sensors at spectral level, the validation of classification accuracies, and the relevance of this fine scale classification, mainly within the built environment. This paper therefore attempted to answer three research questions:

i. How does the unique nature of commercial spaceborne VHR imagery influence their capacity to extract urban land cover classes effectively?
ii. In an unsupervised pixel-based land cover classification procedure, is there a significant variation in accuracy results between three selected VHR sensors?
iii. Is change detection analysis feasible between different VHR sensors and their classification products?

## 2. Study Area, Data and Methods

### 2.1 Study area

To ensure that an assortment of settlement types was included, a diverse area of 15km x 10km in the eastern Tshwane Municipal Area was selected as the overall area of interest (AOI), as illustrated in Figure 1. Other than transport features (roads and railway), the AOI included high and low density residential properties, commercial and industrial zones, open public spaces, quarries and agricultural plots as the dominant land uses.

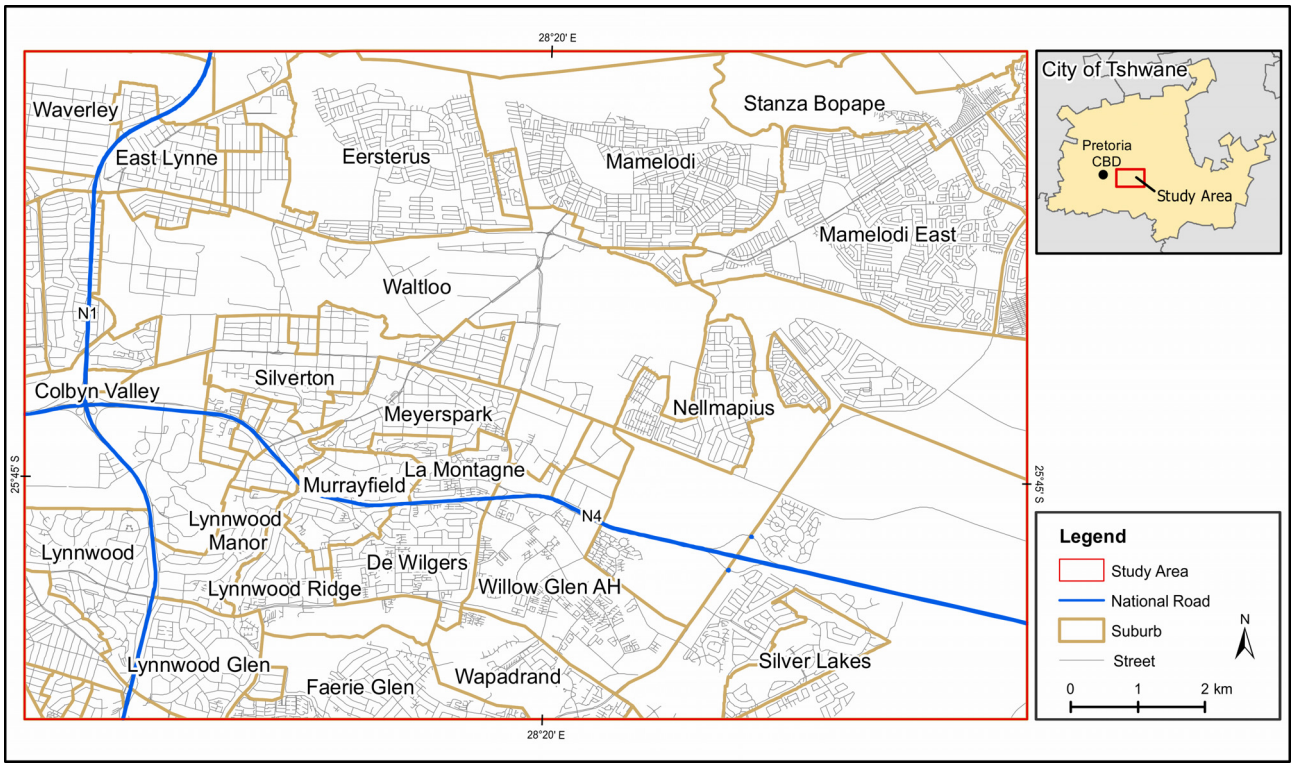


Figure 1: Geographical study area in the City of Tshwane
(Map compiled by the Unit for Geoinformation and Mapping, University of Pretoria)

## 2.2 Data selection and preparation

In this investigation we applied a systematic approach towards the classification of primary land cover classes from a trio of VHR electro-optical satellites, Pléiades, WorldView-2 and RapidEye. Resolution for these sensors ranges between 5m and 2m multi-spectral, representing various spectral bands within the visible to NIR spectrum as illustrated in Figure 2.

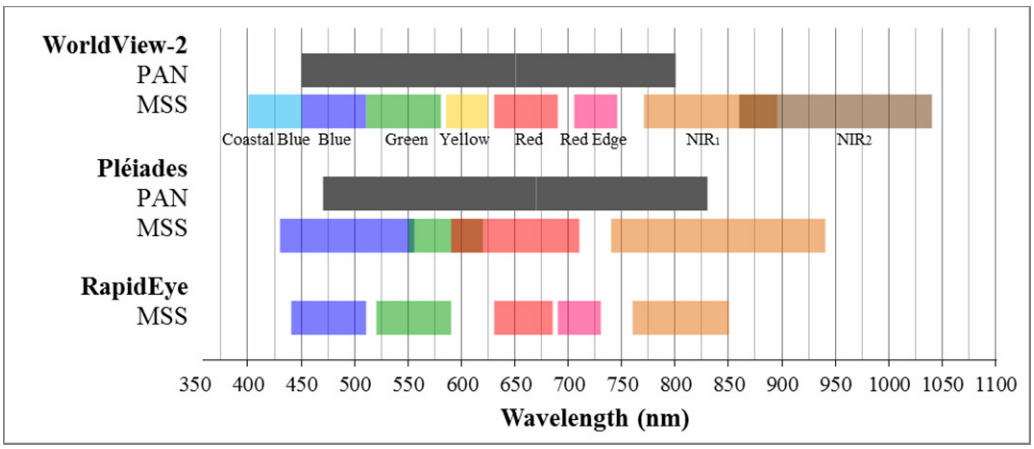


Figure 2: Spectral ranges represented in the band combinations of three VHR satellites

Note the band overlaps within the two top RS platforms (mixed/darker areas in the colour bar) and combinations between all three satellites. The data used were ordered as ortho-rectified imagery directly from the satellite operators. The pre-processing systems used by these satellite operators are well advanced, producing acceptable radiometric as well as geometrical accuracies without ground control points (GCPs). The relevant specifications and accuracies are listed in Table 1, including the particular acquisition dates of each image used.

Table 1: Product specifications and acquisition dates of imagery used

| Sensor | Acquisition Date | Product Resolution (MSS) | Geometric Accuracy (without GCPs) | Pixel Depth |
|---|---|---|---|---|
| WorldView-2 | 11/03/2011 | 2m | 5.0m (CE90)* | 11 bit |
| RapidEye | 22/03/2012 | 5m | 4.6m (CE90) | 12 bit |
| Pléiades | 24/03/2012 | 2m | 3.0m (CE90) | 12 bit |

* Specification at nadir on flat terrain

Subsets encompassing the study area were created to maintain the same analytical geographical extent in all images. The subset area was used to align all three datasets geometrically with each other. A polynomial geo-referencing procedure improved the geometrical registration of all the different images since the original pixel alignment between the images was not acceptable. Due to its superior geometric accuracy (3m), the Pléiades image was used as the master image to co-register the WorldView-2 and RapidEye image using the AutoSync module of the Erdas Imagine software (ERDAS, 2012).

### 2.3 Hierarchical land use classification

Land cover refers to the type of physical cover or feature on the earth's surface, while land use is characterized by the human and/or economic activities associated with a particular area (Lillesand et al., 2004). As introduced in the South African National Land Cover 2000 programme (Van den Berg et al., 2008), classified land cover classes may be converted to land use by applying a typical hierarchical principle (tree structure) to guide the researcher. Figure 3 demonstrates this concept of hierarchical urban land use classification with three primary classes (A1-A3), with only the non-vegetated land cover class (A3) expanded upon towards Level III.

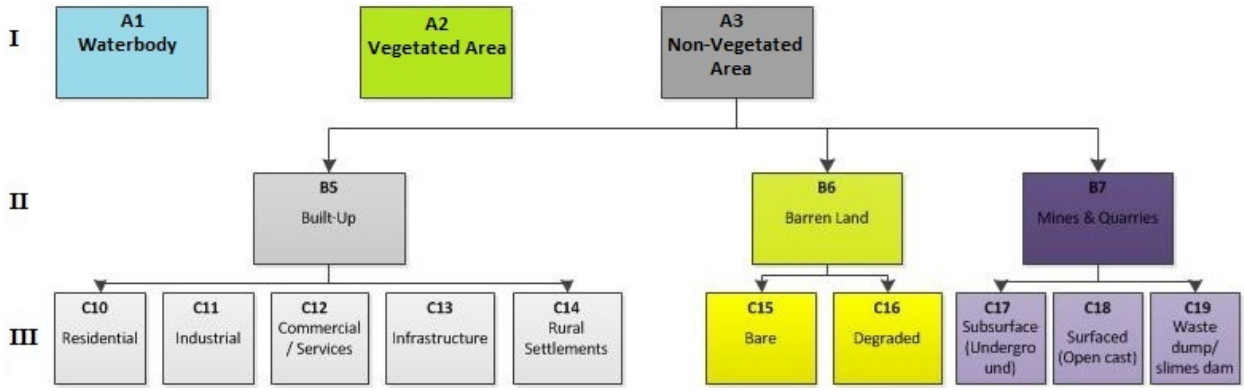


Figure 3: Illustrated example of a possible land cover to land use classification hierarchy for non-vegetated areas in urban and semi-urban environments

In such a land cover tree, Level I represents the primary land cover classes, Level II a further sub-class of land cover and at Level III downwards the associated land use classes.

### 2.4 First stage unsupervised classification using vegetation indices

The primary classes extracted at the onset of this analysis consisted of three land cover types: water, vegetation and non-vegetated areas. The subset area of each image was used to generate a Normalized Difference Vegetation Index (NDVI), a standard RS technique for identifying vegetation. The rationale for this step is to determine the spectral potential of each sensor based on the NIR and Red (R) bands from a standardised algorithm:

$$NDVI = (NIR-R)/(NIR+R) \quad [1]$$

The NDVI result was used to separate water bodies, non-vegetated and completely vegetated areas. The selection of these primary land cover classes in the cases of Pléiades and RapidEye was based on the histogram values generated by the NDVI calculation and the resulting natural breaks that represent specific dominant classes. Water bodies would have a particular negative threshold NDVI value, the remaining negative values up to zero indicate bare earth and impervious surfaces, whereas the positive values indicate that vegetation is present. To fully exploit the eight spectral bands on offer, supplementary investigations into the extraction of the water and non-vegetated

layer from the WorldView-2 image followed multiple NDVI-type calculations using various band combinations as indicated in Table 2.

Table 2: NDVI algorithm used to extract primary land cover classes from the WorldView-2 image using different band combinations

| NDVI function | Associated land cover extracted |
|---|---|
| **RED EDGE & GREEN (1)**<br>(Red Edge – Green)/( Red Edge + Green) | Water body |
| **NIR1 & YELLOW (2)**<br>(NIR1 – Yellow)/(NIR1 + Yellow) | Water body |
| **NIR2 & RED (3)**<br>(NIR2 – Red)/(NIR2 + Red) | Water body |
| **NIR2 & RED EDGE (4)**<br>(NIR2 – Red Edge)/(NIR2 + Red Edge) | Water body & Non-vegetated area |
| **YELLOW & COASTAL BLUE (5)**<br>(Yellow – Coastal Blue)/(Yellow + Coastal Blue) | Non-vegetated area |
| **RED EDGE & RED (6)**<br>(Red Edge – Red)/(Red Edge + Red) | Non-vegetated area |

The selection of the most significant histogram values associated with water and non-vegetated areas was achieved through finding the optimal band combinations in this case. The threshold value for extracting water bodies was -0.33 with lesser values recoded as 1 and the rest as zero. The summation of the results (1+2+3+4) provided a >95% pixel selection over the associated water features when investigated visually. To find the non-vegetated areas, the water body values were recoded as NoData and the remaining pixel values divided into two classes based on the natural breaks (Jenks) algorithm in ArcGIS 10.1 (2012), summed and appropriately recoded (NDVI+4+5+6), as for the water body class before. The remainder then constituted the vegetated areas and, together with the non-vegetated primary land cover classes, served as sub-AOI input layers during the ISODATA classification processes after manual segmentation.

### 2.5 Manual segmentation

In order to improve the interpretation of the pixel based classification, expert knowledge was used in a manual segmentation procedure which in essence ‘clusters’ the spectral values associated with a particular dominant land use, as located within the study area. The unique nature of South African town planning history, with distinctly segregated residential and economic development, simplifies this zoning approach, making it possible to delineate most of the determinant land use classes along major transport routes. A road mask generated in ArcGIS 10.1 (2012) – representing freeways, major roads and streets – further ensured that no pixel classifications over road areas (including traffic) were included during classification. This, in turn, rendered this layer a suitable ‘edge’ when the land cover results within each segment were finally reassembled for the complete study area mosaic. The seven dominant land use zones (polygons) based on the manual segmentation procedure that applied were (1) mining areas, (2) clustered estates (upmarket gated residential areas), (3) residential areas, (4) rural zones, (5) smallholding/agriculture zones, (6) township areas (peripheral underdeveloped urban developments) and (7) industrial areas. After

creating these zones, only the vegetated and non-vegetated land cover classes within each zone type were clipped to produce the final input AOI files for the unsupervised classification routine.

### 2.6 ISODATA Classification and post-processing

Since 'between sensor' quality is the focus of this paper and not a comparison of the various classifiers, the classification technique used was centred on the pixel-based unsupervised ISODATA classification module from the Erdas Imagine 13.0 (2012) image processing software. Unlike the more complicated and time-consuming non-parametric object orientated classifiers, unsupervised classifiers iteratively assign pixels to a selected number of groups (classes) by locating clusters in the data space. Adding meaning (class names) to each group is left to interpretation by the analyst (Adams and Gillespie, 2006). For each of the previously described final AOIs a signature file (based on 48 classes and allowing up to 99 iterations) was produced for each satellite image. The generated signature file was then used in the interpretation and merging of associated classes within each of the final AOIs. The vegetated areas were further divided into short and tall vegetation, while the non-vegetated classes were sub-divided into built-up and bare soil classes. These classification results were imported into a thematic recode function to allocate a specific numeric numbering code per class type. For the WorldView-2 image two coding structures were applied, the original result containing eleven classes (Table 3), and an adjusted result as a comparable structure to the six defined classes (water, built-up, tall vegetation, short vegetation, bare soil and shadows) extracted from the other two sensors.

Table 3: Urban land cover coding and classes used in the study

| Code | Recode | Description | Satellite | Code | Description | Satellite |
|---|---|---|---|---|---|---|
| 0 | 0 | Shadows | WorldView-2 | 0 | Shadows | Pléiades & RapidEye |
| 1 | 1 | Waterbody clear | WorldView-2 | 1 | Water | Pléiades & RapidEye |
| 2 | 1 | Waterbody turbid (bio) | WorldView-2 | 2 | Built-up | Pléiades & RapidEye |
| 3 | 1 | Waterbody turbid (soil) | WorldView-2 | 3 | Tall vegetation | Pléiades & RapidEye |
| 4 | 1 | Swimming pool | WorldView-2 | 4 | Short vegetation | Pléiades & RapidEye |
| 5 | 4 | Short vegetation | WorldView-2 | 5 | Barren soil | Pléiades & RapidEye |
| 6 | 4 | Medium vegetation | WorldView-2 | | | |
| 7 | 3 | Tall vegetation | WorldView-2 | | | |
| 8 | 4 | Cultivated grass | WorldView-2 | | | |
| 9 | 5 | Barren soil | WorldView-2 | | | |
| 10 | 2 | Built-up | WorldView-2 | | | |
| 11 | 2 | Barren/Built-up | WorldView-2 | | | |

Post-processing was necessary to deal with the ambiguous shadow class and the typical 'salt-and-pepper' effect of pixel-based classifiers and VHR imagery. Neighbourhood functions are specialized filtering functions suitable for use on thematic layers (Yee *et al*., 1986; Dost, 2001). After mosaicking the classified AOIs for each of the three sensor types into three resultant image files (one for each sensor) and recoding shadow pixels as NoData, a 5x5 majority filter was run to effectively fill previous shadow cells with adjacent LC classes. The initial LC raster was then mosaicked back on top of this (the target raster) to retain the original class values. Finally a 3x3

majority filter was applied to 'smooth' the classification results by eliminating isolated pixels and very small pixel groups.

### 2.7 Verification and accuracy assessment

For verification of the classification results a stratified random sample was taken of on the classified layers. Fifty-eight point-locations were created by the ArcGIS 10.1 (2012) random point generator using the manually segmented zones as strata. Land cover types as identified by in-situ field observations at a selection of 25 points, and interpreted using Google Earth imagery for the remaining 33 points, were used in combination for the validation process. In the RS environment the actual pixel classification end result is thus compared to the field work observations and often interpreted via confusion matrices (Myburgh and Van Niekerk, 2013). Classification accuracy was calculated per sensor using the well-known Kappa coefficient, as well as overall and class specific accuracy statistics. Frequently exploited to summarize the results of an accuracy assessment used to evaluate land use or land cover classifications derived from RS products (Fitzgerald and Lees, 1994; Kokaly *et al*., 2003; Munyati *et al*., 2013; Sexton *et al*., 2013), Cohen's Kappa (κ) refers to the pair-wise agreement coefficient between two observers who each classify a number of items into a specific number of mutually exclusive categories (Cohen, 1960). This agreement coefficient for each of the three sensors was calculated by using the native Kappa coefficient from the *proc FREQ* procedure in SAS 9.3 (2012).

### 2.8 Change detection analysis

Due to the time difference of just over a year between the WorldView-2 and Pléiades imagery the possibility existed of detecting significant changes that occurred during this period. Image differences were calculated with the "Image Difference" tool available in the Erdas Imagine 13.0 (2012) software, using a parameter setting of 10% increase and decrease values respectively. A post-classification comparison was also performed using the classified Pléiades and RapidEye land cover products, since their acquisition dates were only two days apart and should represent the same land cover scene. To achieve this task, the Pléiades map was first resampled to 5m using a nearest neighbour (NN) algorithm and co-registered (using NN) with the RapidEye raster. Standard GIS and statistical procedures were then used to calculate the correlation between the Pléiades land cover codes with those of RapidEye. The last-mentioned sensor acted as the predictive master raster due to its marginally superior classification accuracy as discussed in the following section that reviews the study results.

## 3. Results and Discussion

This research intended to examine and spatially compare urban land cover information obtained from a systematic routine that classified images from three different optical satellite VHR sensors. Roughly similar to Lu *et al*. (2010), a hybrid method based on stratification, unsupervised pixel based classification and manual editing for mapping urban land cover distribution was implemented

in this study. Additional thematic enhancements, the validation of the overall classification results and land cover differences/changes were explored. Three research questions were stated earlier in this paper and will now form the basis of presenting the results.

i. *How does the unique nature of commercial spaceborne VHR imagery influence their capacity to extract urban land cover classes effectively?*

NDVI derived classification results from all three sensors provided clear differentiation between the three primary classes, *i.e.* water bodies, non-vegetated, and vegetated areas. The manual segmentation approach (to create smaller more homogeneous land use zones) followed by an ISODATA classification contributed to the extraction of four additional subclasses (short and tall vegetation, built-up and bare soil) that, together with water bodies, defined the five fundamental LC classes obtained in this study (Figure 4).

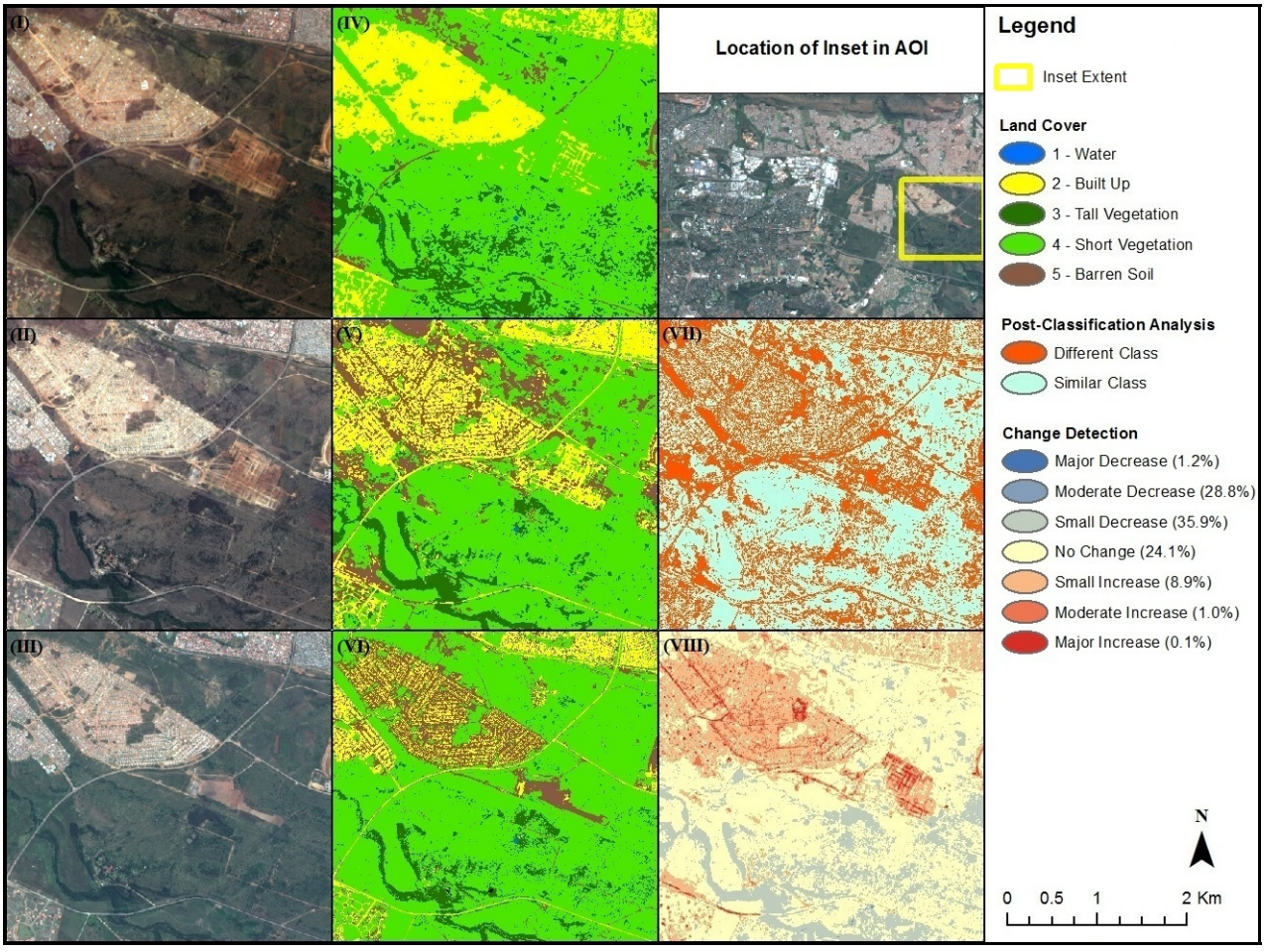


Figure 4: Zoomed in true colour images of (I) RapidEye, (II) Pléiades and (III) WorldView-2, with their respective (IV, V & VI) classified land cover results. Results of (VII) post-classification analysis between Pléiades and RapidEye, and (VIII) image differencing between WorldView-2 and Pléiades are indicative of urban-rural fringe dynamics and some seasonal effects.

The WorldView-2 image, based on its eight bands as input provided a more precise and distinctive visual result compared to Pléiades and RapidEye, especially with the newly introduced coastal and yellow bands. The significance thereof is embedded within its potential to further distinguish a primary class into its relevant sub-classes, as shown by the extended list of detectable classes earlier (Table 3). As close inspection of Figure 4 (VI) will show, noteworthy improvements were made with the accurate classification of certain rooftops or modern building materials as part of the built-up class, due to WorldView-2's additional spectral bands, compared to Pléiades (V) for example.

ii. *In an unsupervised pixel-based land cover classification procedure, is there a significant variation in accuracy results between three selected VHR sensors?*

The 58 validation points generated were geographically well distributed throughout the AOI and well represented within all the different class types except for water bodies, with only one location intersecting a small stream. The classification of the defined land cover classes between the three sensors in question offered an overall good result and was relevant for the built environment domain. As listed by the statistics in Table 4, the sensor with the best overall agreement mainly due to the mentioned 8-band advantages was WorldView-2 (overall accuracy of 0.79 and 0.71κ).

RapidEye results showed a high overall accuracy (0.78) that marginally surpassed the overall result of Pléiades (0.74), notwithstanding the coarser 5m pixel resolution. With regards to the built-up areas alone though, Pléiades delivered the best classification accuracy from both a producer's (93.3%) and consumer's (82.4%) perspective, compared to the other two sensors.

Table 4. Confusion matrices with statistics indicating the class accuracies for three sensors

| **WorldView-2** | **Observed LC Class (Field & Google)** | | | | | | |
|---|---|---|---|---|---|---|---|
| **LC Class** | Water Body | Built-Up | Tall Vegetation | Short Vegetation | Bare Soil | TOTALS | Producer's accuracy (%) |
| Water Body | 1 | 0 | 0 | 0 | 0 | 1 | 100.0 |
| Built-Up | 0 | 12 | 1 | 0 | 4 | 17 | 85.7 |
| Tall Vegetation | 0 | 0 | 9 | 2 | 2 | 13 | 90.0 |
| Short Vegetation | 0 | 0 | 0 | 21 | 0 | 21 | 87.5 |
| Bare Soil | 0 | 2 | 0 | 1 | 3 | 6 | 10.3 |
| TOTALS | 1 | 14 | 10 | 24 | 9 | 58 | |
| User's accuracy(%): | 100.0 | 70.6 | 69.2 | 100.0 | 50.0 | | |
| Overall Accuracy: | 0.79 | | | | | | |
| Overall Kappa: | 0.71 | | | | | | |
| **Pléiades** | | | | | | | |
| Water Body | 0 | 0 | 0 | 1 | 0 | 1 | 0.0 |
| Built-Up | 0 | 14 | 0 | 0 | 3 | 17 | 93.3 |
| Tall Vegetation | 0 | 0 | 10 | 2 | 1 | 13 | 71.4 |
| Short Vegetation | 0 | 0 | 4 | 14 | 3 | 21 | 82.4 |
| Bare Soil | 0 | 1 | 0 | 0 | 5 | 6 | 10.3 |
| TOTALS | 0 | 15 | 14 | 17 | 12 | 58 | |
| User's accuracy(%): | 0.0 | 82.4 | 76.9 | 66.7 | 83.3 | | |
| Overall Accuracy: | 0.74 | | | | | | |
| Overall Kappa: | 0.65 | | | | | | |
| **RapidEye** | | | | | | | |
| Water Body | 0 | 0 | 1 | 0 | 0 | 1 | 0.0 |
| Built-Up | 0 | 13 | 0 | 4 | 0 | 17 | 86.7 |
| Tall Vegetation | 0 | 0 | 12 | 1 | 0 | 13 | 75.0 |
| Short Vegetation | 0 | 0 | 3 | 17 | 1 | 21 | 73.9 |
| Bare Soil | 0 | 2 | 0 | 1 | 3 | 6 | 10.3 |
| TOTALS | 0 | 15 | 16 | 23 | 4 | 58 | |
| User's accuracy(%): | 0.0 | 76.5 | 92.3 | 81.0 | 50.0 | | |
| Overall Accuracy: | 0.78 | | | | | | |
| Overall Kappa: | 0.69 | | | | | | |

*iii. Is change detection analysis feasible between different VHR sensors and their classification products?*

A post-classification comparison at 5m GSD using the classified Pléiades and RapidEye land cover products revealed between them a moderate overall accuracy of 0.59, but poor Kappa coefficient (0.41), as indicated in Table 5.

Table 5. Confusion matrix with statistics indicating the class accuracy between two sensors

| Pléiades | RapidEye LC Class | | | | | | |
|---|---|---|---|---|---|---|---|
| LC Class | Water Body | Built-Up | Tall Vegetation | Short Vegetation | Bare Soil | TOTALS | Producer's accuracy (%) |
| Water Body | 8867 | 377 | 395 | 225 | 1114 | 10978 | 70.0 |
| Built-Up | 2196 | 969483 | 44940 | 167342 | 304475 | 1488436 | 61.8 |
| Tall Vegetation | 906 | 36826 | 743880 | 454443 | 38101 | 1274156 | 66.9 |
| Short Vegetation | 542 | 527657 | 317504 | 1623549 | 459841 | 2929093 | 70.1 |
| Bare Soil | 156 | 34363 | 5074 | 70492 | 167245 | 277330 | 4.6 |
| TOTALS | 12667 | 1568706 | 1111793 | 2316051 | 970776 | 5979993 | |
| User's accuracy(%): | 80.8 | 65.1 | 58.4 | 55.4 | 60.3 | | |
| Overall Accuracy: | 0.59 | | | | | | |
| Overall Kappa: | 0.41 | | | | | | |

Water displayed the best user's accuracy (80.8%), followed by the built-up class (65.1%) and less encouraging results for the rest. From a producers point of view, only water and short vegetation was adequately (>70%) extracted, but typical confusion between the two vegetated classes and between impervious surfaces (61.8%) and bare soil (4.6%) in particular, existed. The overall class agreement – simplified and illustrated in Figure 4 (VII) earlier – disclosed that only about 59% of the classified pixels fully matched within the entire AOI.

Annual change detection by means of image differencing was possible and results highlighted various land cover/land use changes within the study area. Confirming the phenomenon of urban densification, various newly introduced land use activities were identified and matched with the calculated image differences when inspected closely. As depicted in Figure 4 (VIII) earlier, about a quarter of the AOI revealed no significant change, but ten percent (5km$^2$) accounted predominantly for settlement expansions to new industries in the 'increasing' (red) classes. Area-wise the seasonal vegetation adjustments made up almost two thirds of the remaining areas, as represented mainly by the 'decreasing' (blue) class values.

## 4. Conclusion

VHR sensors such as WorldView-2 and Pleiades delivered finer scale accuracy at pixel level when compared to RapidEye. However, RapidEye exhibited excellent potential to extract very useful urban land cover classes if a high-level overview of the larger metropolitan area is required at application level, as opposed to a detailed sub-urban synopsis. If the required result is an accurate fine scale map, then Pléiades and/or WorldView-2 VHR imagery becomes recommendable, with the additional bands available from WorldView-2 proving more versatile when extracting various sub-classes. In this study however, as also noted by Elsharkawy *et al*. (2012), this added capability of WorldView-2 introduced significant uncertainty (noise) at a pixel-based classification level. Because of its fine spectral distinction between specific spectral values, it may cause an impervious (built-up) surface to end up in the "Bare Soil" class, or *vice versa* – a common confusion in RS classification. These challenges may be addressed through enhanced segmentation techniques and/or GEOBIA (Fröhlich, *et al*., 2013), since by simply adding texture to objects (Martinfar *et al*., 2007) higher accuracy potential can be attained. The selection between these three sensors remains

an assessment of the detail required within the application/deliverable, as well as the financial investment available.

## 5. References


Adams, JB & Gillespie, AR 2006, *Remote sensing of landscapes with spectral images : a physical modeling approach,* Cambridge, UK; New York, Cambridge University Press.

Aguilar MA, Vicente R, Aguilar FJ, Fernández A & Saldaña MM 2012, 'Optimizing object-based classification in urban environments using very high resolution GeoEye-1 imagery', *ISPRS Annals of the Photogrammetry, Remote Sensing and Spatial Information Sciences,* vol. I-7, pp. 99-104.

Alexakis, DD, Hadjimitsis, DG, Agapiou, A, Themistocleous, K & Retalis A 2012, 'Monitoring urban land cover using satellite remote sensing techniques and field spectroradiometric measurements: case study of "Yialias" catchment area in Cyprus'. *Journal of Applied Remote Sensing*, vol. 6, pp. 1-14.

ArcGIS 10.1 2012, ESRI (Environmental Systems Resource Institute). ESRI, Redlands, California.

Baraldi, A, Wassenaar, T & Kay, S 2010, 'Operational performance of an automatic preliminary spectral rule-based decision-tree classifier of spaceborne very high resolution optical images', *IEEE Transactions on Geoscience and Remote Sensing*, vol. 48 no. 9, pp. 3482-3501.

Biehl, L & Landgrebe, D 2002, 'MultiSpec – a tool for multispectral-hyperspectral image data analysis', *Computers and Geosciences*, vol. 28, pp. 1153–1159.

Bouziani, M, Goita, K & He, D 2010, 'Rule-Based Classification of a Very High Resolution Image in an Urban Environment Using Multispectral Segmentation Guided by Cartographic Data', *IEEE Transactions on Geoscience and Remote Sensin*g, vol. 48 no. 8, pp. 3198-3211.

Brito, PL & Quintanilha, JA 2012, 'A literature review, 2001-2008, of classification methods and inner urban characteristics identified in multispectral remote sensing images', *Proceedings of the 4th GEOBIA*, Rio de Janeiro, Brazil, 7-9 May 2012, pp. 586-591.

Cohen, J 1960, 'A coefficient of agreement for nominal scales', *Educational and psychological measurement,* vol. 20**,** pp. 37-46.

Dost, R 2001, 'Spatial Data Analysis: neighbourhood and connectivity calculations', in Nijmeijer, R & Budde, P (eds.). *ITC-ILWIS*. *IlWIS 3.0 User-guide,* viewed on 26 April 2013, <ftp://ftp.itc.nl/pub/ilwis/ilwis30/pdf/chap09.pdf>.

Elsharkawy, A, Elhabiby, M & El-Sheimy, N, 2012, 'New combined pixel/object-based technique for efficient urban classification using WorldView-2 data', *International Archives of the Photogrammetry, Remote Sensing and Spatial Information Sciences*, vol. XXXIX-B7, pp. 191-195.

ERDAS IMAGINE 13.0, 2012, Intergraph Corporation, Huntsville, AL, USA.

Fichera, CR, Modica, G & Pollino, M 2012, 'Land cover classification and change-detection analysis using multi-temporal remote sensed imagery and landscape metrics', *European Journal of Remote Sensing*, vol. 45, pp. 1-18.

Fitzgerald, RW & Lees, BG 1994, 'Assessing the Classification Accuracy of Multisource Remote Sensing Data', *Remote Sensing of Environment,* vol. 47**,** pp. 362-368.

Fröhlich, B, Bach, E, Walde, I, Hese, S, Schmullius, C & Denzler, J 2013, 'Land cover classification of satellite images using contextual information', *ISPRS Annals of the Photogrammetry, Remote Sensing and Spatial Information Sciences*, vol. II-3/W1, pp. 1-6.

Gholami, R, Moradzadeh, A & Yousefi, M 2012, 'Assessing the performance of independent component analysis in remote sensing data processing', *Journal of the Indian Society of Remote Sensing*, vol. 40 no. 4, pp. 577–588.

Heinl, M, Walde, J, Tappeiner, G & Tappeiner, U 2009, 'Classifiers vs. input variables - The drivers in image classification for land cover mapping', *International Journal of Applied Earth Observation and Geoinformation*, vol. 11, pp. 423-430.

Huth, J, Kuenzer, C, Wehrmann, T, Gebhardt, S, Tuan, VQ & Dech, S 2012, 'Land cover and land use classification with TWOPAC: towards Automated Processing for Pixel- and Object-based Image Classification', *Remote Sensing*, vol. 4, pp. 2530-2553.

Jackson, BB 1983, *Multivariate Data Analysis*, R.D. Irwin, Homewood, Illinois, USA.

Kennedy, RE, Townsend, PA, Gross, JE, Cohen, WB, Bolstad, P, Wang, YQ & Adams, P 2009, 'Remote sensing change detection tools for natural resource managers: understanding concepts and tradeoffs in the design of landscape monitoring projects', *Remote Sensing of Environment*, vol. 113, pp. 1382–1396.

Kokaly, RF, Despain, DG, Clark, RN & Livo, KE 2003, 'Mapping vegetation in Yellowstone National Park using spectral feature analysis of AVIRIS data', *Remote Sensing of Environment,* vol. 84**,** pp. 437-456.

Lillesand, TM, Kiefer, RW & Chipman, JW 2004, *Remote Sensing and Image Interpretation,* USA, John Wiley & Sons.

Li, Q, Tao, Li, Q, Tao, J, Hu, Q & Liu, P 2013, 'Decision fusion of very high resolution images for urban land-cover mapping based on Bayesian network', *Journal of Applied Remote Sensing*, vol. 7, pp. 1-16.

Lu, D, Mausel, P, Brondízio, E & Moran, E 2004, 'Change detection techniques', *International Journal of Remote Sensing*, vol. 25, pp. 2365–2407.

Lu, D, Hetrick, S, Moran, E & Li, G 2010, 'Detection of urban expansion in an urban-rural landscape with multitemporal QuickBird images', *Journal of Applied Remote Sensing*, vol. 23, no. 4, pp. 1-17.

Lu, D & Weng, Q 2007, 'A survey of image classification methods and techniques for improving classification performance', *International Journal of Remote Sensing*, vol. 28, pp. 823-870.

Martinfar, HR, Sarmadian, F, Alavi Panah, SK & Heck, RJ 2007, 'Comparisons of object-oriented and pixel-based classification of land use/land cover types based on Lansadsat7, Etm+ spectral bands (Case study: Arid region of Iran)', *American-Eurasian J. Agric. & Environ,* vol. 2**,** p. 448.

Moran, EF 2010, 'Land Cover Classification in a Complex Urban-Rural Landscape with Quickbird Imagery', *Photogrammetric Engineering and Remote Sensing,* vol. 76 no. 10 pp. 1159–1168.

Muchoney, DM & Haack, BN 1994, 'Change detection for monitoring forest defoliation', *Photogrammetric Engineering and Remote Sensing*, vol. 60, pp. 1243 - 1251.

Munyati, C 2004, 'Use of principal component analysis (PCA) of remote sensing images in wetland change detection on the Kafue Flats, Zambia', *Geocarto International*, vol. 19 no. 3, pp. 11-22.

Munyati, C, Ratshibvumo, T & Ogola, J 2013, 'Landsat TM image segmentation for delineating geological zone correlated vegetation stratification in the Kruger National Park, South Africa', *Physics and Chemistry of the Earth, Parts A/B/C,* vol. 55–57**,** pp. 1-10.

Myburgh, G, Van Niekerk, A 2013, 'Effect of Feature Dimensionality on Object-based Land Cover Classification: A Comparison of Three Classifiers', *South African Journal of Geomatics*, vol. 2, no. 1, pp. 13-27.

Richards, JA 1999, *Remote Sensing Digital Image Analysis,* Springer-Verlag, Berlin, Germany, p 240.

Serra, P, Pons, X & Saurí, D 2003, 'Post-classification change detection with data from different sensors: some accuracy considerations', *International Journal of Remote Sensing*, vol. 24 no. 16, pp. 3311–3340.

Salehi, B, Zhang, Y, Zhong, M & Dey, V 2012, 'Object-based classification of urban areas using VHR imagery and height points ancillary data', *Remote Sensing*, vol. 4, pp. 2256-2276.

SAS 9.3 2012, SAS Institute Inc., Cary, NC, USA.

Sexton, JO, Urban, DL, Donohue, MJ & Song, C 2013, 'Long-term land cover dynamics by multi-temporal classification across the Landsat-5 record', *Remote Sensing of Environment,* vol. 128**,** pp. 246-258.

Thunig, H, Wolf, N, Naumann, S, Siegmund, A, Jürgens, C, Uysal, C & Maktav, D 2011, 'Land use/land cover classification for applied urban planning - The challenge of automation' in Stilla, U, Gamba, P,

Juergens, C, Maktav, D (Eds) JURSE 2011, *Joint Urban Remote Sensing Event*, Munich, Germany, April 11-13, pp. 229-232.

Tehrany, MS, Pradhan, B & Jebuv, MN 2013, 'A comparative assessment between object and pixel-based classification approaches for land-use/land-cover mapping using SPOT 5 imagery', *Geocarto International,* DOI: 10.1080/10106049.2013.768300.

Tou, JT & Gonzalez, RC 1974, 'Pattern Recognition Principles', *Applied Mathematics and Computation*, vol.1, Addison-Wesley Publishing Company, Reading, Massachusetts.

Van Den Berg, EC, Plarre, C, Van Den Berg, HM & Thompson, MW 2008, 'The South African National Land Cover 2000. Final report for the National Land Cover 2000 Funding Consortium', *Project No. GW 51/037 and Project No. GW/A/2008/86.* Summary Report ed.: Agricultural Research Council (ARC) Council for Scientific and Industrial research (CSIR) - Institute for Soil, Climate and Water.

Wurm, M, Taubenböck, H, Roth, A & Dech, S 2009, ' Urban structuring using multisensoral remote sensing data: By the example of the German cities Cologne and Dresden', *Proceedings of Joint Urban Remote Sensing Event*, Shanghai, China, 20-22 May, pp. 1-8.

Xiang, M, Hung, C, Pham, M, Kuo, B & Coleman, T 2005, 'A parallelepiped multispectral image classifier using genetic algorithms', *Proceedings of IEEE Geoscience and Remote Sensing Symposium (IGARSS)*, vol. 1, Seoul, Korea, 25-29 July, pp. 482-485.

Yee, B, Turpin, D, Kenk, E & Sondheim, M 1986, 'A context based technique for smoothing of digital thematic maps', *Canadian Conference on Vision Interface (VI)*, 1986, Canada. Canadian Image Processing and Pattern Recocnition Society (CIPPRS), pp. 279-283.